J. Fluid Mech. (1993), *vol.* 246, *pp.* 43–66

Experimental investigation of capillarity effects on surface gravity waves: non-wetting boundary conditions

By BRUNO COCCIARO[1], SANDRO FAETTI[1] AND CRESCENZO FESTA[2]

[1] Dipartimento di Fisica dell' Universita' di Pisa and Gruppo Nazionale di Struttura della Materia del CNR and Istituto Nazionale di Fisica della Materia, Piazza Torricelli 2, 56100 Pisa, Italy

[2] Dipartimento di Chimica e Chimica Industriale dell' Universita' di Pisa and Gruppo Nazionale di Struttura della Materia del CNR and Istituto Nazionale di Fisica della Materia. Via Risorgimento, 56100 Pisa, Italy

(Received 21 February 1992 and in revised form 23 June 1992)

Damping and eigenfrequencies of surface capillary–gravity waves greatly depend on the boundary conditions. To the best of our knowledge, so far no direct measurement has been made of the dynamic behaviour of the contact angle at the three-phase interface (fluid–vapour–solid walls) in the presence of surface oscillation. Therefore, theoretical models of surface gravity–capillary waves involve *ad hoc* phenomenological assumptions as far as the behaviour of the contact angle is concerned. In this paper we report a systematic experimental investigation of the static and dynamic properties of surface waves in a cylindrical container where the free surface makes a static contact angle $\theta_c = 62°$ with the vertical walls. The actual boundary condition relating the contact angle to the velocity of the contact line is obtained using a new stroboscopic optical method. The experimental results are compared with the theoretical expressions to be found in the literature. Two different regimes are observed: (i) a low-amplitude regime, where the contact line always remains at rest and the contact angle oscillates during the oscillation of the free surface; (ii) a higher-amplitude regime, where the contact line slides on the vertical walls. The profile, the eigenfrequency and the damping rate of the first non-axisymmetric mode of the surface gravity waves are investigated. The eigenfrequency and damping rate in regime (i) are in satisfactory agreement with the predictions of the Graham-Eagle theory (1983) of pinned-end edge conditions. The eigenfrequency and damping rate in regime (ii) show a strongly nonlinear dependence on the oscillation amplitude of the free surface. All the experimental results concerning regime (ii) can be explained in terms of the Hocking (1987*a*) and Miles (1967, 1991) models of capillary damping by introducing an 'effective' capillary coefficient λ_{eff}. This coefficient is directly obtained for the first time in our experiment from dynamic measurements on the contact line. A satisfactory agreement is found to exist between theory and experiment.

1. Introduction

The methods for calculating the eigenfrequencies and damping coefficients of standing capillary–gravity waves in a closed basin for a low-viscosity fluid are well known (see, for instance, Lamb 1932, chapter 9; Case & Parkinson 1957). Standard

theoretical approaches assume that the free surface intersects the vertical walls orthogonally and the contact line at the three-phase interface (solid, liquid and air) can freely slip (*free-end edge condition*) (Ursell 1952; Case & Parkinson 1957).

Experiments have been performed to measure the damping rate of gravity–capillary waves (Case & Parkinson 1957; Keulegan 1959; Van Dorn 1966; Benjamin & Ursell 1954). In most of these experiments the damping rate is found to be higher than the theoretical value predicted for free-end edge conditions. Either contamination of the free surface by a thin impurity layer or effects of meniscus at the vertical walls were proposed to explain discrepancies between theory and experiment (Miles 1967). In particular, measurements of damping rates of progressive wave using controlled films at the free surface for wetting boundary conditions showed that contamination of the free surface can cause a strong increase in the damping rate (Davies & Vose 1965). Furthermore Case & Parkinson showed that the damping rate approaches the free-end value after careful polishing of the internal walls of the container. In order to explain certain experimental results, Benjamin & Scott (1979) and Graham-Eagle (1983, 1984) make the assumption that, in some cases, the contact line can remain at rest even in the presence of oscillation of the free surface. This new boundary condition is known as the *pinned-end edge condition*. More recently Hocking (1987*a*) and Miles (1967, 1991) proposed a new and more general boundary condition where the macroscopic contact angle is assumed to be a linear function of the velocity of the contact line. The free-end and the pinned-end edge conditions represent two different limiting cases for this new boundary condition. Hocking showed that all previous experimental results could be explained by a proper choice of the capillary coefficient λ which characterizes the boundary condition. However, the dynamic behaviour of the contact line was not investigated in previous experiments and, thus, a quantitative comparison between experimental results and theoretical modes is not possible.

This brief discussion shows that a complete experimental investigation of the dynamic properties of surface waves requires a careful analysis of the dynamic properties of the contact line. In this paper we report new experimental results concerning the low-amplitude regimes of surface capillary–gravity waves for a low-viscosity fluid (water) in an oscillating cylindrical container. The shape, damping rate and eigenfrequency of the fundamental non-axisymmetric surface mode are investigated in detail by means of an optical apparatus. The dynamic behaviour of the contact angle and contact line is investigated during surface oscillation in order to establish the boundary conditions which best describe the actual behaviour of the system. This measurement allows us to closely correlate the dynamic properties of surface waves with those of the meniscus and, for the first time, makes direct comparison between theory and experiment possible.

In a previous paper (Cocciaro, Faetti & Nobili 1991) we investigated the behaviour of surface waves when the fluid (octane or water) wets the vertical walls ($\theta_c = 0$). In this case the main behaviour of the system was found to be close to the predictions of the free-end theory of surface waves although certain small deviations from the theory were observed.

In the present experiment we investigate capillary–gravity waves in the case of a fluid (water) which makes a macroscopic static contact angle of $\theta_c = 62°$ with the vertical walls of a cylindrical Plexiglas container. The experimental behaviour of surface waves with these boundary conditions appears to be completely different as compared to the previous case ($\theta_c = 0$).

In order to understand this behaviour, we performed a direct measurement of the

contact angle and of the position of the contact line during the oscillation of the free surface. This measurement allowed us to obtain the first direct measurement of the Hocking capillary coefficient λ. Depending on the maximum displacement A of the free surface, two different regimes were found: *a small oscillation amplitudes regime* ($A < A^c$), where the contact line remains at rest and the macroscopic contact angle oscillates around its static value. The damping of the first non-axisymmetric surface mode is characterized by a small *constant* damping rate, whilst the eigenfrequency is almost 200 mHz higher than the free-end theoretical value (≈ 3 Hz). This regime can be explained in terms of the pinned-end edge condition; (ii) a higher-amplitude regime ($A > A^c$), where the contact line slides on the walls. In this regime the damping coefficient greatly increases with the oscillation amplitude until it reaches a maximum value and, then, decreases (*nonlinear damping*). The maximum value of the damping rate is more than ten times greater than that measured in the case of regime (i). The oscillation eigenfrequency tends to approach the value predicted by the free-end theory as the oscillation amplitude increases. Our experimental results are in satisfactory quantitative agreement with the predictions of a theoretical model based on the Miles (1967, 1991) and Hocking (1987*a*, *b*) boundary conditions. To the best of our knowledge this is the first direct experimental observation of the regime of capillary nonlinear damping which was predicted by Miles (1967). Furthermore our experimental results are the first measurements of the behaviour of the contact angle in the presence of the oscillation of the free surface (see Miles 1990; Miles & Henderson 1990).

2. Theoretical models of capillary–gravity waves

2.1 *Models of free-end and pinned-end edge conditions*

The oscillation of the free surface for the first non-axisymmetric longitudinal mode of an inviscid fluid with free-end edge conditions can be written as (Ursell 1952; Case & Parkinson 1957):

$$\eta(r, \theta, t) = \eta_1(t) J_1(k, r) \cos\theta, \tag{2.1a}$$

where

$$k_1 = \frac{1.8412}{a}, \tag{2.1b}$$

where r and θ are planar polar coordinates (θ is the angle with a horizontal x-axis), J_1 is the Bessel function of integer order $n = 1$, a is the radius of the cylindrical tank and $\eta_1(t)$ is an oscillating function of time with an angular frequency ω_1 given by:

$$\omega_1 = \left[g k_1 \left(1 + \frac{T}{\rho g} k_1^2 \right) \tanh k_1 h \right]^{\frac{1}{2}}, \tag{2.2}$$

where h is the depth of the fluid, g is the acceleration due to gravity, T is the surface tension and ρ is the mass density.

For a low-viscosity fluid with free-end boundary conditions, (2.1*a*) remains substantially correct except in a very thin viscous boundary layer near the interfaces of the fluid. Viscosity has two main effects on fluid motion: it produces a damping of free surface waves and a small change in their eigenfrequencies. Here we define damping rate γ as the coefficient which occurs in the expression of the decay of surface oscillations: $\eta(t) = \eta_0 \exp(-\pi\gamma t)$. At the first order in the small dimensionless parameter:

$$\epsilon = \left(\frac{2\nu_c k_1^2}{\omega_1} \right)^{\frac{1}{2}}, \tag{2.3}$$

the viscous damping coefficient γ_w for the first non-axisymmetric mode is determined by dissipation near the walls and is given by (see, for instance, Case & Parkinson 1957):

$$\gamma_w = \frac{\omega_1 \epsilon}{4\pi}\left[0.998 + 2\left(1-\frac{h}{a}\right)\operatorname{cosech}\left(\frac{3.682\,h}{a}\right)\right], \tag{2.4}$$

whilst the angular eigenfrequency is given by (Mei & Liu 1973):

$$\omega_1 = \left[g k_1 \left(1+\frac{T}{\rho g}k_1^2\right)\tanh k_1 h\right]^{\frac{1}{2}} - \pi\gamma_w, \tag{2.5}$$

where ν_c is the kinematic viscosity of water.

All previous results were deduced by assuming that surface gravity waves must obey free-end edge conditions. However, conventional boundary conditions (free-end) may not correspond to the actual ones. In particular, in most experiments, the contact angle θ_c between the fluid–air interface and the vertical walls may not be 90° and, thus, a meniscus occurs at the contact line. Furthermore certain experiments (Dussan, V. 1979) seem to indicate that the contact line may also remain at rest in the presence of a fluid motion (pinned-end edge condition). It has been shown that this new boundary condition ($\eta(a) = 0$ at the vertical walls) suitably describes the edge constraint for a rim-full container (Benjamin & Scott 1979; Graham-Eagle 1983, 1984; Douady 1988, 1989).

Benjamin & Scott conjecture that the edge constraint $\eta(a) = 0$ may hold good for a container that is not rim-full. However, there is a large body of experimental evidence (see, for instance, Ablett 1923; Dussan, V. 1979; Dussan V., Ramé & Garaff 1991) indicating that the behaviour of the contact line is much more complex. According to the Young–Laplace equation, the macroscopic contact angle should be fixed and equal to θ_c in static conditions. However, experiments indicate that a range of possible static angles, centred on the Young–Laplace angle, may exist (*capillary hysteresis*). This static range is exceeded when the contact line moves.

2.2 *Theories of linear capillary damping*

In recent papers, Hocking (1987*a*, *b*) has proposed a new phenomenological linear boundary condition which might partially simulate the complex behaviour of a real fluid–solid interface. To make theoretical analysis possible, Hocking makes the simplifying assumptions that the static contact angle is 90° (flat unperturbed free surface), that the hysteresis of the contact angle is not present and the dynamic contact angle is a linear function of the velocity of the contact line. The proposed 'wetting' boundary condition is:

$$\frac{\partial\eta(a,\theta,t)}{\partial t} = \lambda'\frac{\partial\eta(a,\theta,t)}{\partial \boldsymbol{n}}, \tag{2.6}$$

where $\eta(a,\theta,t)$ is the displacement of the free surface at the vertical wall of the cylindrical basin ($r = a$) and at time t, $\boldsymbol{n}$ is the inwardly directed normal to the vertical wall and λ' is a phenomenological capillary coefficient. Hocking implicitly assumes λ' is a real number. The free-end and the pinned-end edge conditions can be obtained as borderline cases for $\lambda' = \infty$ and $\lambda' = 0$, respectively. Using this new boundary condition Hocking calculated both the eigenfrequencies and the damping rates of the surface capillary–gravity waves in a rectangular channel for a low-viscosity fluid. By assuming suitable values for the capillary coefficient λ', Hocking obtained a plausible agreement with the experimental results reported by Benjamin & Ursell (1954), Case & Parkinson (1957) and Keulegan (1959). Unfortunately, in all

previous experiments the dynamics of the contact line was not investigated and, thus, the agreement between theory and experiment can only be qualitative.

In a recent paper, Miles (1991) generalizes the Hocking model by assuming that the λ'-coefficient in (2.6) is a complex number. Miles restricts his analysis to the simplest case of an inviscid fluid in both the cases of a cylindrical and a rectangular tank. The essential non-dimensional parameters of the problem are:

$$k = k_1 \lambda_c, \quad \lambda = \frac{\lambda'}{\omega \lambda_c}, \tag{2.7a, b}$$

where λ coincides with the parameter γ introduced by Miles and

$$\lambda_c = \left(\frac{T}{\rho g}\right)^{\frac{1}{2}} \tag{2.7c}$$

is the capillary length which is $\lambda_c \approx 2.7$ mm for pure water at room temperature. Experimental measurements of λ do not appear to be available, while theoretical considerations suggest that $|\lambda| \ll 1$ for harmonic motion (Miles 1990). Disregarding static meniscus, Miles obtained an 'exact eigenvalue equation' for the eigenfrequency for both rectangular and cylindrical containers. Theoretical results coincide with those obtained by Hocking in the case of a rectangular channel and with the results obtained by Graham-Eagle (1983) for a cylindrical container with pinned-end edge conditions ($\lambda = 0$). In order to obtain analytical expressions for eigenfrequencies and damping rates, Miles considers the borderline case $k \to 0$, retaining only contributions of the first order in the small parameter k (boundary-layer approximation). In these conditions he also shows that corrections due to the presence of static meniscus are of a higher order than the first order in the perturbation parameter k (Miles 1990). Therefore, for $k \ll 1$, theoretical predictions are also expected to be sufficiently accurate for $\theta_c \neq 90$. At the first order in the small parameter k, the displacement of the free surface with respect to the static profile is given by:

$$\eta(r, \theta, t) = \eta(t)\left[J_1(k_1 r) - \frac{1}{1 - i\lambda} \exp\left(-\frac{a - r}{\lambda_c}\right) J_1(k_1 a)\right] \cos\theta, \tag{2.8}$$

where i represents the imaginary unity. For small oscillation amplitudes of the free surface, the time-dependence of the contact angle at the vertical walls along the direction $\theta = 0$ is:

$$\theta_c(t) = \theta_c - \left.\frac{\partial \eta(r, \theta = 0, t)}{\partial r}\right|_{r=a} = \theta_c + \frac{1}{(1 - i\lambda)} \frac{A(t)}{\lambda_c}, \tag{2.9}$$

where θ_c is the static contact angle and $A(t) = \eta(t) J_1(k_1 a)$. The angular eigenfrequency ω' is related to the free-end edge value ω_1 of (2.2) by:

$$\frac{\omega'^2 - \omega_1^2}{\omega_1^2} = \frac{2.84 \lambda_c}{(1 - i\lambda) a} + O(k^2), \tag{2.10}$$

where $O(k^2)$ is a small contribution of the order k^2. In our experiment the radius of the cylinder is $a = 50.25$ mm, $\lambda_c = 2.7$ mm and the non-dimensional parameter k for the first non-axisymmetric mode is $k = 0.099$. Therefore, the first-order approximation is expected to be appropriate for the analysis of our experimental results. In particular for $\lambda = 0$, the ratio ω'/ω_1 as predicted from the boundary-layer approximation (equation (2.10)) is $\omega'/\omega_1 = 1.0736$ which is virtually coincident with the value $\omega'/\omega_1 = 1.0737$ which is obtained by numerically solving the exact eigenvalue equation (equation (4.5) in Miles 1991). The oscillation eigenfrequency ν'

and the capillary damping rate γ_L are related to the real and the imaginary part of ω'. According to the following experimental results, we can assume that capillary coefficient λ is a real number and, thus, by exploiting the condition $\lambda_c \ll a$ in (2.10) we find:

$$\gamma_L = \frac{\omega_i'}{\pi} \approx \frac{0.452\lambda\lambda_c\omega_1}{(1+\lambda^2)a}, \tag{2.11a}$$

$$\nu' = \frac{\omega_r'}{2\pi} \approx \nu_1\left[1+\frac{1.42\lambda_c}{(1+\lambda^2)a}-\frac{\gamma_L^2}{8\nu_1^2}\right], \tag{2.11b}$$

where ω_r' and ω_i' are the real and the imaginary part of ω', respectively, and $\nu_1 = \omega_1/2\pi$. Note that the capillary damping coefficient vanishes in the two borderline cases $\lambda = 0$ and $\lambda = \infty$.

In the presence of a small value of viscosity, the damping coefficient and the eigenfrequency become (Hocking 1987*a*):

$$\gamma = \gamma_L + \gamma_v, \quad \nu = \nu' - \tfrac{1}{2}\delta_v, \tag{2.12a, b}$$

where γ_v and δ_v depend on λ and k. The influence of a small but not vanishing value of viscosity was investigated by Hocking (1987*a*) for a rectangular channel. For $k \ll 1$, γ_v and δ_v approach the free-end values $\gamma_v = \delta_v = \gamma_w'$ except in the special case $\lambda \approx 0$ where $\gamma_v \approx 0.67\gamma_w'$. Here γ_w' denotes the viscous damping rate for a rectangular channel with free-end boundary conditions.

So far we have not taken into consideration the possible presence of a thin impurity film on the free surface. Previous experiments (Davies & Vose 1965; Scott 1981) and theoretical works (Miles 1967) clearly show that contamination of the free surface significantly affects both the damping rate and the eigenfrequency. In particular it has been found that variations of surface tension of less than 5 dyn/cm from the clean surface value can cause a great increase in the damping rate. According to Miles (1967) the contribution of the thin surface film to the damping rate is:

$$\gamma_s = C\frac{\omega_1\epsilon}{4\pi}\coth k_1 h, \tag{2.13}$$

where C is a coefficient which depends on the viscoelastic properties of the surface film: $C = 1$ for an inextensible film and ranges for a minimum value $C = 0$ to a maximum value $C = 2$. Equation (2.13) has been deduced by assuming free-end edge conditions and by disregarding terms of a higher order than ϵ. For deep water ($k_1 h \gg 1$) and in the case of an inextensible film ($C = 1$), the damping coefficient γ_s of (2.13) is virtually coincident with the viscous damping coefficient γ_w of (2.4). Therefore the presence of an inextensible film is expected to produce a doubling of the damping rate due to viscosity in agreement with experiments (Davies & Vose 1965; Scott 1981). We emphasize that all mechanisms so far discussed are intrinsically linear mechanisms which give damping coefficients (equations (2.4), (2.11*a*) and (2.13)) and eigenfrequencies which do not depend on the oscillation amplitude of the free surface.

2.3. *Theory of nonlinear capillary damping*

Boundary condition (2.6) holds good if the contact angle is a linear function of the contact line velocity and no capillary hysteresis is present. Experiments seem to indicate that the real behaviour at the liquid–wall interface may be strongly nonlinear (capillary hysteresis). The possible effect of the nonlinear behaviour of the dynamic contact angle on the damping of surface gravity waves was investigated theoretically some years ago by Miles (1967) using a different theoretical approach.

Here we briefly describe the main results that we obtain by following a different procedure which allows us to generalize the Miles' results concerning the damping rate and to obtain new theoretical results for the eigenfrequency. A justification of this approach and a comparison with Miles' results is given in Appendix A. The starting point is the capillary boundary condition (2.6) where the coefficient λ is not a constant coefficient but is assumed to be a function of the velocity v of the contact line. As shown in the Appendix, the main effects of this new boundary condition can be accounted for by introducing an effective capillary coefficient λ_{eff} which is given by the average value of $\lambda(v)$ over an oscillation period. The eigenfrequency and the damping rate of the first non-axisymmetric mode are still approximately given by (2.11*a*, *b*) if one substitutes λ_{eff} for λ. According to Miles (1967) and to our experimental results, we consider the case where the capillary coefficient λ is a linear function of the absolute value of v and the velocity of the contact line is a sine function of time. In this case we find:

$$\lambda_{\text{eff}} = \langle \lambda \rangle = \langle D|v| \rangle = \frac{2D\omega A_{\text{c}}}{\pi}, \tag{2.14}$$

where D is a constant coefficient, A_{c} is the oscillation amplitude of the contact line and $\langle\ \rangle$ denotes the average value over an oscillation period. By putting λ_{eff} given by (2.14) in the place of λ in (2.11*a*, *b*), we find a theoretical expression for the capillary damping coefficient which depends on the oscillation amplitude A_{c} and approaches the Miles value (1967) in the limit $\lambda \to \infty$. Note that both γ_{L} and ν' are no longer constant coefficients but depend on the oscillation amplitude A_{c}. This is the very special feature of the nonlinear damping model compared to the previous models of linear damping where both the damping rate and the eigenfrequency were independent of the oscillation amplitude.

3. Experiment

3.1 *Apparatus and experimental procedures*

The experimental set-up used to generate the oscillation of the cylindrical tank and to measure the surface displacement of the free surface is shown in figure 1. This apparatus is the same as that used by Nobili *et al.* (1988) to investigate the chaotic behaviour of surface gravity waves and it is similar to that used by Douady (1988, 1989).

The fluid (bi-distilled water) is contained in a Plexiglas cylindrical tank of radius $a = 50.25$ mm. The internal surfaces of the Plexiglas container are cleaned by gentle scrubbing with anionic detergent (DECONTAMIN, Inter Sciences SA) and, then, by rinsing with clean bi-distilled water. No suctioning procedure is used to remove contaminant particles from the free surface except in the case of damping rate measurements (see §3.4). All the experiments are performed with depth $h = 130$ mm for the fluid ($h \gg a$; deep water). The oscillation of the cylindrical container in figure 1 is produced by a 150 W loudspeaker (L). The local displacement $\eta(r, \theta, t)$ of the free surface is detected by using the method outlined in figure 1. A laser beam (LB) impinges orthogonally on the bottom of the container, then is refracted by the free surface of the fluid and, finally, is collected by a dual-axis position-sensitive photodetector (PP). The photodetector gives two output signals (V_x and V_y) that are proportional to the displacement of the laser spot on the photosensitive surface of the photodetector with respect to its centre along two orthogonal axes x and y (x is the oscillation axis of the carriage). Then these signals, for small values of η, are

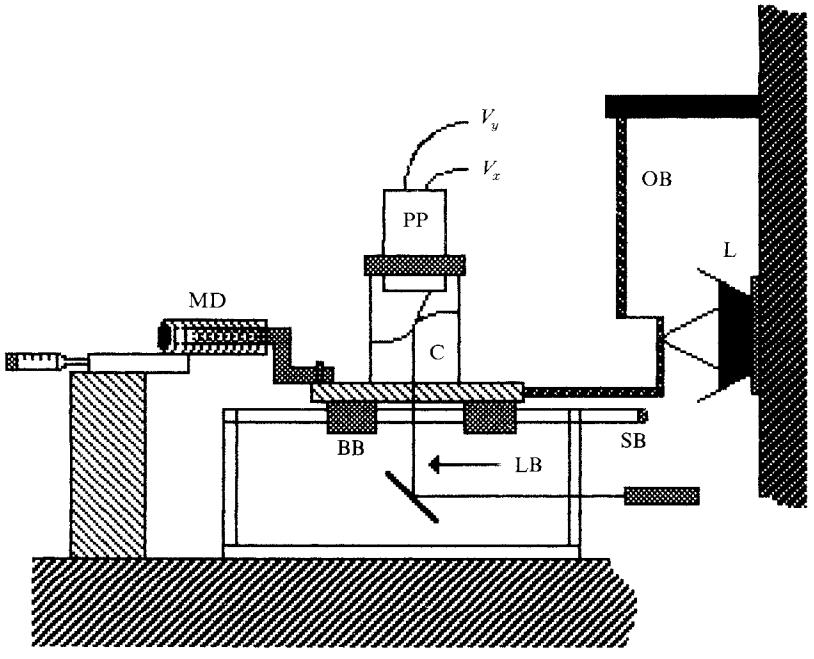

FIGURE 1. Sketch of the experimental apparatus. L = loudspeaker; OB = brass bar; SB = stainless-steel bars; LB = laser beam; BB = ball-bearings; MD = electromagnetic device to measure carriage displacement; C = cylindrical container; PP = position-sensitive photodetector.

proportional to the spatial derivatives $\partial\eta/\partial x$ and $\partial\eta/\partial y$ at the incidence point of the laser beam. By changing the incidence point we can reconstruct the surface deformation η at each point of the free surface by integrating the output signals with respect to the x- and y-coordinates. This method can only be used to investigate the free-surface displacement far from the meniscus. Indeed, if the laser beam impinges on the free surface very close to the meniscus, the refracted beam crosses the vertical walls of the cylindrical container and cannot be collected by the photodetector. The surface profile near the vertical walls is obtained by measuring the reflection angle of a laser beam which impinges on the free surface from the top.

In our experiment the power of the laser beam was set to 0.5 mW and no appreciable variation of the damping rate and of the eigenfrequency of the fundamental mode was measured when the laser power was increased up to 3 mW. Therefore heating effects of the laser beam are negligible in our experimental conditions.

The static and dynamic behaviour of the meniscus at the vertical walls is investigated using the optical set-up shown in figure 2. A He–Ne laser beam is focused by the objective O (60 cm focal length) on a small region (200 μm width) of the meniscus. The laser beam is refracted by the fluid wedge and impinges on a horizontal screen S at a distance x from the vertical wall. The laser can be moved along the vertical z-axis by means of a micrometric translator. When the laser spot on the free surface reaches the contact line (C in figure 2), it suddenly splits into two divergent transmitted laser beams which correspond to optical rays which impinge over and below the contact line, respectively. Then, the vertical position h_c of the contact line can be obtained by reading on the micrometric screw the vertical displacement of the laser beam. Optical rays which pass above the contact line are not refracted, whilst those which pass below the contact line are refracted by the fluid

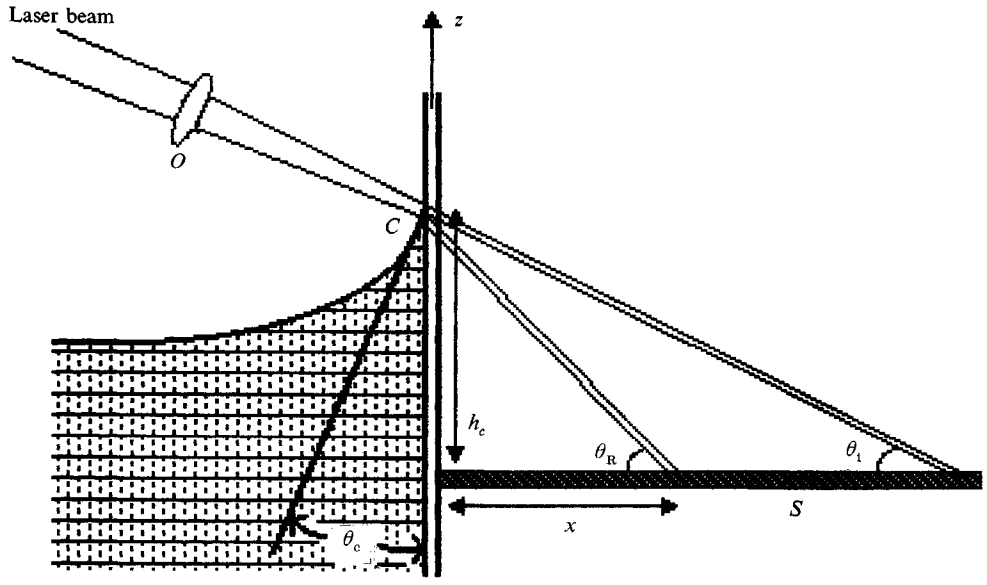

FIGURE 2. Sketch of the optical set-up used to measure the static and the dynamic behaviour of the contact line, C, and of the contact angle θ_c. The He–Ne laser beam is focused on the meniscus by means of a 60 cm-focal length objective. The beam width at the meniscus is $\Delta = 200$ μm. The laser beam is refracted from the meniscus and impinges on the horizontal screen S at distance x from the vertical wall of the cylindrical container. h_c is the height of the contact line with respect to the horizontal screen S.

wedge. By measuring the position of the two laser spots on the screen S, we obtain the angles θ_i and θ_R which the incident and the refracted beams make with the horizontal plane, respectively. The macroscopic contact angle θ_c is related to θ_i and θ_R by the expression:

$$\tan\theta_c = \frac{\sin\theta_i - \sin\theta_R}{\cos\theta_i - (n^2 - \sin^2\theta_R)^{\frac{1}{2}}}, \tag{3.1}$$

where n is the refractive index of the fluid ($n = 1.33$ for water). The accuracy of the measurement of the contact angle is $\pm 1°$.

The same experimental method is used to investigate the dynamic behaviour of the contact angle and of the contact line when the cylindrical tank is subjected to horizontal oscillation. In this case, however, a stroboscopic technique is used since both the contact angle and the vertical position of the contact line change periodically with time. The intensity of the laser beam is periodically modulated by means of an optical shutter which generates periodic laser pulses at the same repetition frequency as the oscillator with a duration time smaller than 1 ms, that is about $\frac{1}{300}$ of the period T_0. The retardation time ΔT of the pulses with respect to the oscillator which drives the cylindrical tank can be continuously changed. The unperturbed position $d = 0$ of the contact line can be established by moving the laser beam along the vertical axis until the refracted beam fully disappears when the free surface does not oscillate. This means that the spot of the laser beam remains just above the static contact line. By repeating the same procedure when the free surface oscillates and using the stroboscopic lightening at a given retardation time ΔT, we can then measure the corresponding vertical displacement $d(\Delta T)$. The estimated accuracy of this measurement is of the order of $\Delta d = \pm 100$ μm. Then, by putting the spot of the laser beam just below the position of the contact line at time $t = \Delta T$, we

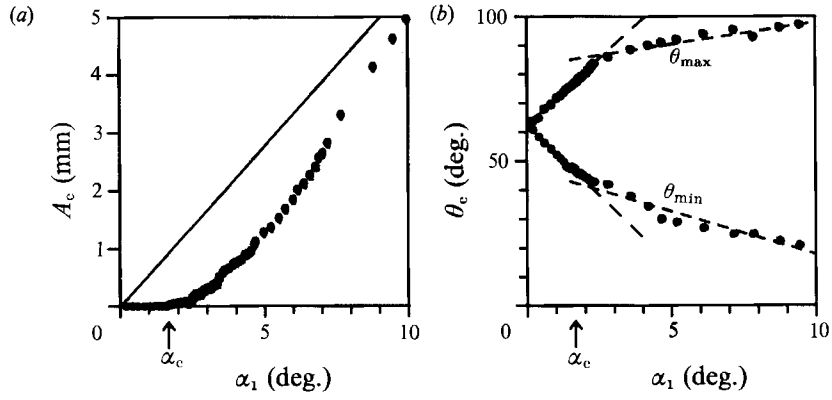

FIGURE 3. (*a*) Oscillation amplitude A_c of the contact line versus the amplitude α_1 of the first harmonic component of the tilt angle at the centre of the free surface. The oscillation amplitude of the contact line is measured where the excitation x-axis intersects the vertical wall ($\theta = 0$ in (2.1*a*)). (*b*) **Maximum and minimum dynamic contact angle versus the amplitude α_1 of the first harmonic component of the tilt angle at the centre of the free surface. These angles are measured at the point where the excitation x-axis intersects the vertical wall ($\theta = 0$ in (2.1*a*)). ●, experimental results obtained by increasing the oscillation amplitude of the cylindrical tank. ——, oscillation amplitude predicted by the free-end edge conditions. The cylinder radius is $a = 50.25$ mm, the height of the fluid is $h = 13$ cm and the oscillation frequency corresponds to the experimental value of the resonance frequency of the first non-axisymmetric mode at very small oscillation amplitudes ($\nu = 3.220$ Hz). α_c is the threshold amplitude for the sliding of the contact line.

can measure the contact angle $\theta_c(\Delta T)$. The accuracy of the measurement of the contact angle in this regime is estimated to be $\pm 3°$.

3.2. *Dynamic properties of the meniscus*

If the cylindrical tank is subjected to a monochromatic horizontal oscillation of amplitude x_0 and of a frequency close to the resonance frequency of the first non-axisymmetric mode, two main regimes occur depending on the amplitude x_0. At small oscillation amplitudes, below a critical value x_0^c, the contact line remains at rest and the contact angle oscillates between a minimum value θ_{min} and a maximum value θ_{max}. Above the threshold x_0^c, the contact line starts to slide and the oscillation amplitude A_c of the contact line is an increasing function of x_0. The threshold amplitude x_0^c greatly depends on the oscillation frequency of the cylindrical tank and, thus, it is not a significant parameter as far as this system is concerned. The most relevant parameter in this experiment is the maximum oscillation amplitude of the free surface which is proportional to the oscillation amplitude of the tilt angle α at the centre of the free surface. Indeed, by repeating measurements at different frequencies close to the resonance of the first non-axisymmetric mode, we find that the transition to the motion of the capillary line always occurs at the same critical tilt angle α_c.

Figure 3(*a*) shows the oscillation amplitude A_c of the contact line versus the amplitude α_1 of the first harmonic component of the tilt angle α of the free surface at the centre ($\alpha = \partial\eta/\partial x|_{x=0,y=0}$). Amplitude α_1 is measured by sending the x-output of the position-sensitive photodiode in figure 1 to the input channel of a digital waveform analyser (Data Precision–Data 6100) and by making the Fourier analysis of the signal. The oscillation amplitude of the contact line is measured at the point where the excitation x-axis intersects the vertical wall ($\theta = 0$ and $r = a$ in (2.1*a*)). The dots in figure 3(*a*) represent the experimental results obtained by increasing the

Number of mode	α_c (exp.)	α_c (the.)
1	1.8 ± 0.3	1.4 ± 0.15
2	7.5 ± 1.5	6.6 ± 0.7
3	14 ± 3	13.4 ± 1.4
4	19.5 ± 4	21.6 ± 2.2

TABLE 1. Experimental and theoretical values of the threshold tilt angles for the first four non-axisymmetric modes.

oscillation amplitude of the cylinder. The same results are obtained, within the limits of experimental uncertainty of 10–15%, in the case of decreasing oscillation amplitudes. At the critical tilt angle $\alpha_c = 1.8° \pm 0.3°$, the contact line starts to slide. Owing to the experimental uncertainty $\Delta d = \pm 100$ μm on the displacement of the contact line, the experimental value of the critical tilt angle is affected by a great uncertainty $\Delta\alpha_c \approx \pm 15\%$. The full line in figure 3(*a*) represents the theoretical prediction for the oscillation amplitude of the contact line when the surface mode is given by a Bessel function (see (2.1)) and, thus:

$$A_c = \frac{2J_1(k_1 a)}{k_1} \frac{\partial \eta}{\partial r}\bigg|_{r=0,\theta=0} = 0.011 a \alpha_1, \tag{3.2}$$

where α_1 is expressed in degrees and a is the radius of the cylindrical basin. Note that the experimental values of A_c always remain below the theoretical full line and tend to approach it as the oscillation amplitude of the free surface is increased. This behaviour agrees with the predictions in (2.8) if we assume (as confirmed by the following experimental results) that the capillary coefficient λ is not constant but greatly increases as the tilt angle α_1 increases.

Figure 3(*b*) shows the maximum and minimum values of the dynamic contact angles versus α_1 for increasing oscillation amplitudes of the cylinder. The critical tilt angle α_c in figure 3(*a*) is also indicated in the figure. We see that the difference between the maximum contact angle θ_{max} and the minimum angle θ_{min} is an increasing function of α_1 which shows a change of slope close to the critical tilt angle $\alpha_1 = \alpha_c$. The broken lines in figure 3(*b*) are guide-lines for the reader's convenience.

To understand the physical meaning of the threshold α_c, we investigated the behaviour of the first four non-axisymmetric surface modes. The qualitative behaviour of the contact line and of the contact angle in these cases is analogous to that observed in the case of the first excited mode (see figure 3), although the noise of the experimental data is greater. In particular, the maximum and minimum values of the contact angle at the critical angle α_c are the same as in figure 3(*b*) within the limits of experimental uncertainty of 3%, whilst the value of the critical tilt angle α_c is an increasing function of the number n of the mode. Column 2 in table 1 shows the experimental values of the threshold tilt angles α_c for the first four non-axisymmetric modes. The accuracy and reproducibility of the critical angles is estimated to be 15%. The experimental results in table 1 can be explained if we make the assumption that the contact line remains at rest until the contact angle becomes lower than a minimum allowed value $\theta_{min} \approx 47°$ or greater than a maximum value $\theta_{max} \approx 79°$. These angles correspond to the values measured at the critical tilt angle α_c. When the contact angle exceeds this static range, the contact line cannot remain at rest and starts to slide on the vertical walls. When the nth mode is excited and the

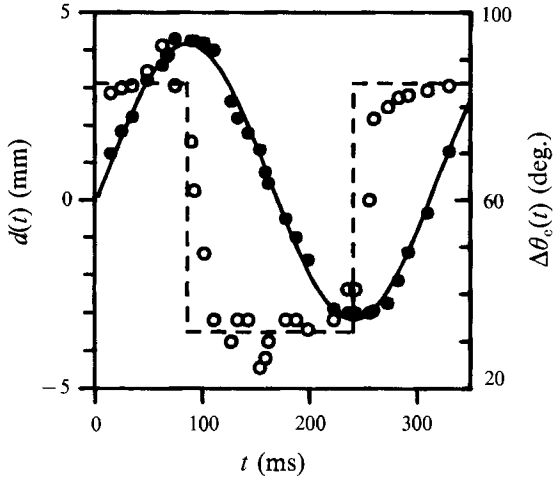

FIGURE 4. ●, displacement $d(t)$ of the contact line and ○, variation $\Delta\theta_c(t) = \theta_c(t) - \theta_c$ of the contact angle at time t when the oscillation amplitude of the tilt angle at the centre of the free surface is $\alpha_1 = 8.3°$. The horizontal displacement of the tank is maximum at $t = 224$ ms. The left-hand scale corresponds to $d(t)$ whilst the right-hand scale corresponds to $\Delta\theta_c(t)$. The other relevant parameters of the experiment are the same as in figure 3 (*a*). ——, best fit of the experimental points concerning $d(t)$ to the sine-function: $d(t) = A + B \sin(\omega t + \phi)$ where A, B and ϕ are free parameters: $A = 0.50$ mm, $B = 3.67$ mm and $\phi = 10.5°$. Angular eigenfrequency ω is fixed to be $\omega = 20.29$ rad/s. – – –, square-wave signal which roughly approximates the actual behaviour of the contact angle.

contact line is at rest, the free-surface displacement can be described by using the Miles capillary model with $\lambda = 0$. According to Miles (1991), the free-surface displacement is still represented by (2.8) with $\lambda = 0$ where k_1 must be replaced by the wavevector k_n of the nth non-axisymmetric longitudinal mode (see also the full line in figure 6). In this regime, according to (2.8), the oscillation amplitude α_1 of the tilt angle at the centre of the free surface is proportional to the oscillation amplitude $\Delta\theta_c$ of the contact angle. The contact line starts to slide as soon as the contact angle exceeds the static range ($\Delta\theta_c > \frac{1}{2}(\theta_{max} - \theta_{min})$). By using the theoretical expression in (2.8) for $\lambda = 0$ with k_n in place of k_1 and by accounting for the condition $\lambda_c \ll a$, we find:

$$\alpha_1 = \frac{k_n \lambda_c \Delta\theta_c}{2|J_1(k_n a)|}. \tag{3.3}$$

The threshold for the sliding of the contact line is reached when $\Delta\theta_c$ exceeds the static range, that is:

$$\alpha_1 \geqslant \alpha_c = \frac{k_n \lambda_c (\theta_{max} - \theta_{min})}{4|J_1(k_n a)|}. \tag{3.4}$$

In our experiment for all surface modes we find $\theta_{max} - \theta_{min} \approx 32° \pm 3°$ for $\alpha_1 = \alpha_c$. By substituting this value in (3.4) together with the value $\lambda_c = 2.7$ mm for pure water, we find the theoretical values of α_c given in column 3 of table 1. A satisfactory agreement between the measured and the calculated values is found to exist if we account for the large experimental uncertainties on α_c (experimental) ($\approx 15\%$) and α_c (theoretical) ($\approx 10\%$).

The stroboscopic method in figure 2 allows us to measure the displacement $d(t)$ of the contact line and the variation $\Delta\theta_c(t) = \theta_c(t) - \theta_c$ of the contact angle at each time t. The experimental values of $d(t)$ (solid dots) and $\Delta\theta_c(t)$ (open dots) for $\alpha_1 = 8.3°$ are shown in figure 4. The-left-hand scale corresponds to $d(t)$ and the right-hand scale to $\Delta\theta_c(t)$. The time at which the displacement of the tank reaches its maximum value

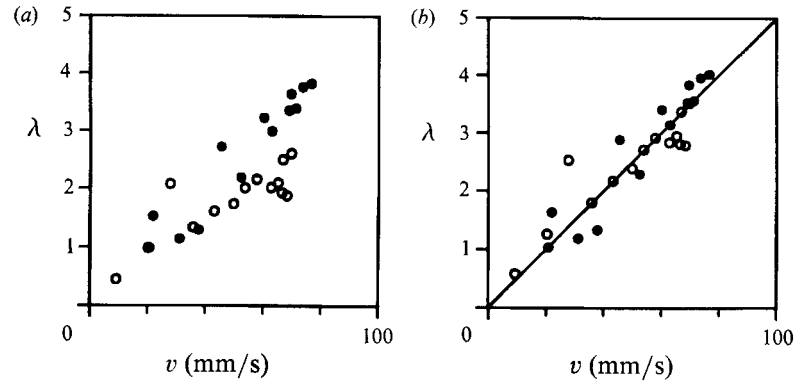

FIGURE 5. (*a*) Dependence of the capillary coefficient $\lambda = v/(\omega\lambda_c D\theta_c)$ versus the modulus $|v|$ of the velocity of the contact line. (*b*) Dependence of the capillary coefficient $\lambda = v/[\omega\lambda_c(\cos\theta_c(t) - \cos\theta_c)]$ versus the modulus $|v|$ of the velocity of the contact line. ●, experimental results concerning advancing ($v > 0$) and ○, receding ($v < 0$) contact lines. ——, best fit of the experimental points to the linear dependence $\lambda = D|v|$, where $D = 0.5 \pm 0.05$ s/cm.

is $t = 244$ ms. The oscillation period is $T_0 = 0.3095$ s. The solid line in figure 4 represents the best fit of the experimental points concerning $d(t)$ with the sine-function: $d(t) = A + B\sin(\omega t + \phi)$. The displacement $d(t)$ of the contact line is virtually sinusoidal but its average value $d = A = 0.7$ mm does not coincide with the unperturbed value $d = 0$. The variation $\Delta\theta_c(t)$ of the contact angle shows a periodic but non-sinusoidal time-dependence. Therefore the linear boundary condition in (2.6) is not appropriate for the description of our experimental results. A better approximation to the present experimental results seems to be provided by the Miles (1967) nonlinear boundary condition (see (A 3) in the Appendix). In particular, the time-variation of the contact angle in figure 4 can be roughly approximated by a square wave signal with $\theta_a \approx 85°$ for the advancing contact line and $\theta_t \approx 32°$ for the receding contact line. The broken line in figure 4 represents a square-wave signal which roughly approximates the actual behaviour of the contact angle. It is interesting to note that the velocity $v(t)$ of the contact line and the contact angle $\theta_c(t)$ are *in-phase periodic signals*. This means that the boundary condition which connects $v(t)$ and $\theta_c(t)$ can be represented by (2.6) with a *real but not constant* capillary coefficient λ. The same kind of measurements were repeated for different oscillation amplitudes and give similar results. In particular it is important to observe that the displacement of the contact line is always well represented by a sine-function of time even for values of α_1 which slightly exceed the critical value α_c.

The experimental results in figure 4 allow us to investigate the actual boundary condition at the macroscopic contact line. Indeed, from figure 4 we can obtain both the velocity $v(t)$ of the contact line and the variation $\Delta\theta_c(t)$ of the contact angle and, thus, we can calculate the capillary coefficient defined by (see (2.7*b*) and (2.6)):

$$\lambda = \frac{v}{\omega\lambda_c \Delta\theta_c}. \tag{3.5a}$$

Figure 5(*a*) shows coefficient λ versus the modulus of velocity $|v|$. The solid and open dots denote experimental results for the advancing ($v > 0$) and receding ($v < 0$) contact lines, respectively. Although a large spread of experimental results can be clearly seen in figure 5(*a*), we observe that λ is not a constant coefficient but it increases versus $|v|$ and that there is an asymmetry between results concerning the

advancing and receding contact lines. In particular the solid dots are systematically above the open dots. This asymmetry can be understood if we note that the capillary coefficient in (3.5*a*) has been defined by making the assumption that $\Delta\theta_c \ll 1$, whilst, in our experiment, $\Delta\theta_c \approx 1$. According to the Miles model of nonlinear damping (see the Appendix), one might expect (A 3), rather than (2.6), to be a better approximation to the correct boundary condition for high values of $\Delta\theta_c$. This means that the capillary coefficient λ should be defined by:

$$\lambda = \frac{v}{\omega\lambda_c[\cos\theta_c(t) - \cos\theta_c]}. \tag{3.5b}$$

Using this new expression for λ we find the dependence shown in figure 5(*b*). In this case the asymmetry of the experimental results concerning the advancing and receding contact lines is removed. Within the limits of experimental uncertainty, λ can be represented by a linear function of $|v|$. The full line in figure 5(*b*) represents the best fit of experimental data to the linear dependence $\lambda = D|v|$ where $D = 0.5 \pm 0.05$ s/cm. Similar results are obtained by repeating the same kind of measurement for different values of the oscillation amplitude of the cylindrical container if $\alpha_1 > \alpha_c$: within the limits of experimental uncertainty, we always find $\lambda = D|v|$. Therefore in our experiment the *linear* Hocking capillary regime (λ = const) is never observed except in the pinned-end case ($\lambda = 0$).

3.3 *Static properties of surface waves*

Surface properties of fluids depend on the surface tension T of the free surface. For bi-distilled water at room temperature, the surface tension is considerable ($T = 72$ dynes/cm) and greatly decreases if the free surface is contaminated by impurities. Therefore it is important to control surface tension during experiments. This is done by measuring the reflection angle of a laser beam impinging on the free surface from the top at different points along the x-axis. The reflection angle is related to the local tilt angle of the free surface. According to the theory of capillarity, the tilt angle shows an exponential dependence on the distance from the vertical wall with a characteristic length λ_c. In fresh water samples we find $\lambda_c = 2.70 \pm 0.05$ mm which corresponds to a surface tension $T = 71.5 \pm 3$ dynes/cm, in agreement with known experimental values. This kind of measurement is repeated continuously during the experiment. Both the characteristic length λ_c and the static contact angle are found to be slowly decreasing functions of time. In particular surface tension is reduced to about 67 dynes/cm after about 24 h, whilst no appreciable variation is found during the first hour.

The dynamic profile of the free surface is characterized by the oscillation amplitude $\eta_0(x)$ of the free-surface displacement $\eta(x,t)$ ($\eta(x,t) = \eta_0(x)\,e^{-i\omega t}$), where x denotes the distance from the centre of the free surface along the excitation axis x. The oscillation amplitude $\eta_0(x)$ is measured by using a laser beam which impinges on the free surface from the top. The laser beam impinges on the free surface at a given point x and the reflected beam is collected by the position-sensitive photodiode. The photodiode can be continuously moved along the x-axis by means of a precision micrometric translator until the output signal becomes zero. This occurs when the spot of the laser beam is at the centre of the active area of the photodiode. Therefore, by measuring the corresponding displacement of the micrometric translator and using the other relevant geometric parameters of the experiment, we can obtain the static reflection angle and, thus, the static tilt angle of the free surface at each point x. In order to use this procedure to obtain the tilt angle, the distance between the free

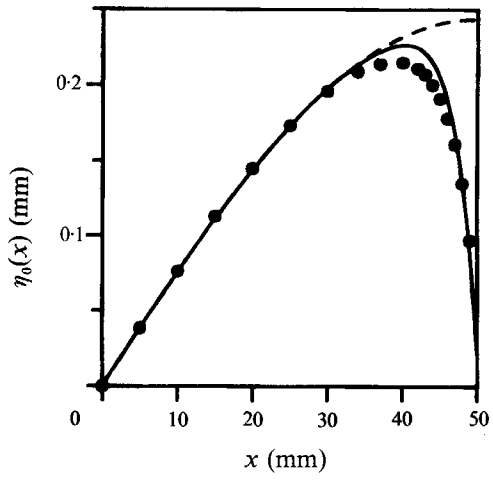

FIGURE 6. Oscillation amplitude $\eta_0(x)$ of the vertical displacement of the free surface versus the distance x from the centre of the free surface when the oscillation amplitude of the tilt angle at the centre of the free surface is $\alpha_1 = 0.44°$ ($\alpha_1 < \alpha_c$). ——, theoretical dependence given by (2.8) when the tilt angle at the centre of the free surface, is $\alpha_1 = 0.44°$ and $\lambda = 0$. No free parameter is used to draw the full line. – – –, the Bessel contribution only in (2.8).

surface and the photodetector needs to be known. In our experiment the distance of the photodetector from the centre of the free surface is $L = 10$ cm and, thus, errors due to the displacement of the mean water level from the horizontal quiescent level can be neglected for small-amplitude waves. The oscillation amplitude of the free surface at point x is obtained by switching on the loudspeaker and by measuring the amplitude of the consequent oscillating output signal of the photodiode. For small oscillation amplitudes, the amplitude of the first harmonic of the x-output signal of the photodiode is proportional to the local value of the derivative $\partial\eta_0/\partial x$ through a coefficient which depends solely on known geometric parameters. Therefore, by moving the laser beam along the x-axis, we can measure both the static local tilt angle and its oscillation amplitude versus the x-coordinate. Integration of the experimental tilt angles with respect to x gives both the static surface displacement $\eta_s(x)$ and the oscillation amplitude of the surface displacement $\eta_0(x)$. In order to use this integration procedure an integration constant needs to be known. This constant can be obtained from the analysis of the experimental data by imposing that the average surface level must coincide with the static one, owing to the incomprimibility of water. In the special case where the contact line remains at rest ($\alpha_1 < \alpha_c$), the unknown integration constant is obtained by imposing $d = 0$ at the walls. The experimental values of $\eta_0(x)$ obtained for $\alpha_1 = 0.44° \ll \alpha_c$ are shown in figure 6. Dots mark the experimental results, whilst the solid line represents the theoretical predictions of the boundary-layer approximation (equation 2.8)) for $\lambda = 0$. No free parameter is used to draw the solid line. The broken line represents the Bessel contribution in (2.8) only. Small deviations of the experimental points from the theoretical behaviour close to the maximum are probably related to second-order contributions in k which were disregarded in (2.8) ($k = k_1 \lambda_c \approx 0.1$ in our experiment). It was not possible to investigate the behaviour of the surface displacement above the threshold α_c because, in this regime, the oscillation amplitude of the reflected beam close to the contact line became very high and exceeded the measurement range of our apparatus.

In order to investigate the influence of the boundary conditions on the surface

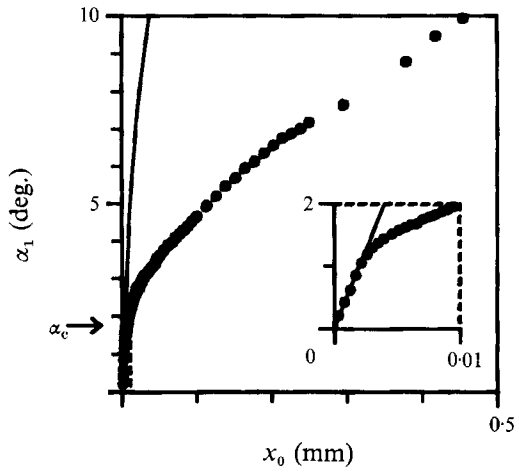

FIGURE 7. Amplitude of the first harmonic component of the tilt angle at the centre of the free surface versus the amplitude of oscillation of the cylindrical container. ——, prediction of the theory for free-end edge conditions. α_c is the threshold value in figure 3(*a*). The cylinder radius is $a = 50.25$ mm, the height of the fluid is $h = 13$ cm and the oscillation frequency is $\nu = 3.220$ Hz. Details of the behaviour close to critical tilt angle α_c are shown in the insert.

waves we measured the dependence of the tilt angle at the centre of the free surface on the oscillation amplitude x_0 of the cylindrical tank. The cylindrical tank was forced at the frequency $\nu = 3.220$ Hz (the resonance frequency of the low-amplitude regime where the contact line is at rest). Figure 7 shows the amplitude of the first harmonic component α_1 of the tilt angle at the centre of the free surface versus x_0 for increasing amplitudes. The behaviour of α_1 below the critical angle α_c is shown in the insert in figure 7. The solid line in figure 7 represents the theoretical value of the tilt angle versus x_0 as predicted by the free-end theory for a damping coefficient $\gamma = 18$ mHz and for $\nu = 3.220$ Hz when nonlinear contributions in the Lagrangian of surface waves are considered (Miles 1984). Note that the nonlinear behaviour of experimental points in figure 7 occurs when the oscillation amplitude of the tilt angle at the centre of the free surface is still much lower than that where the free-end theory predicts the occurrence of significant nonlinearities owing to the coupling of the fundamental mode with higher-order modes (Miles 1984). Therefore the nonlinear behaviour in figure 7 seems to be closely related to nonlinear capillary effects occurring at the boundaries.

3.4. *Damping and eigenfrequencies of surface gravity waves*

To assess the influence of capillary boundary effects on the dynamic properties of surface gravity waves, we measured damping rate γ and eigenfrequency ν of the first resonant mode as a function of the oscillation amplitude. The damping rate and eigenfrequency of capillary–gravity waves in water are known to be greatly sensitive to very small amounts of contaminating particles on the free surface. It has been demonstrated that the distilling process is not sufficient to completely remove surface active particles from water and that the fallout of dust particles from the air is likely to be significant over an hour. Therefore measurements of damping rates and eigenfrequencies require a special treatment of the free surface and a short measurement time. Scott (1981) and Davies & Vose (1965) showed that suction of surface contaminants by using a clean glass capillary attached to a jet pump greatly reduces surface contamination.

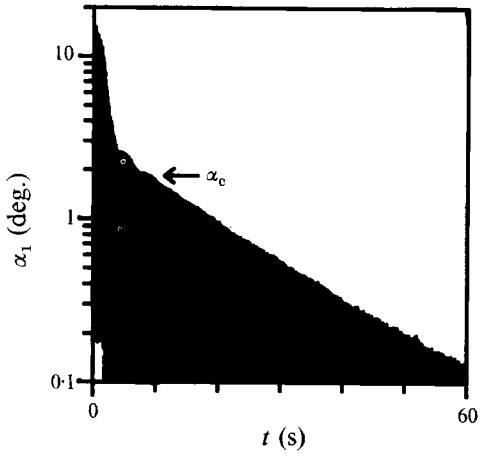

FIGURE 8. Modulus of the amplitude α_1 of the first harmonic component of the tilt angle at the centre of the free surface versus time in a logarithmic scale when the forcing is switched off. We note the linear dependence for $t > 5$ s when the oscillation amplitude of the tilt angle becomes lower than the threshold value. This linear dependence means that the decay of surface oscillations for $t > 5$ s is well represented by a single exponential function.

Our measurements of damping rate and eigenfrequency have been performed using high-purity bidistilled water (Baker Analyzed HPLC for high performance liquid chromatography) and by suctioning the free surface according to the Scott (1981) procedure. Furthermore the duration of measurement was less than 5 min in order to avoid contamination from dust particles in the air. All of the water used passed the sensitive shaking test (Kitchener & Cooper 1959). The surface oscillation is excited at the frequency $\nu = 3.020$ Hz and, then, the carriage oscillation is stopped when the electric oscillating signal which drives the loudspeaker crosses the zero level. The damped oscillation of the tilt angle at the centre of the free surface is measured by means of the apparatus in figure 1. The output signal of the position-sensitive photodetector is sent to a digital waveform analyser and filtered by means of a 24 db electronic filter to reduce noise and harmonic components. Then, a single decay signal is recorded. The response-time of the electronic filter is less than 0.2 s which is negligible compared to the characteristic damping times in our experiment. The logarithm of the modulus of the experimental signal versus time t is shown in figure 8. The damping signal is recorded starting from ≈ 0.5 s after the carriage oscillations stop. We clearly see that the damping rate greatly depends on time and, thus, on the oscillation amplitude of the free surface. At the smallest amplitudes ($\alpha < \alpha_c$), the damping is well represented by a single exponential decay (constant slope in figure 8), whilst at higher amplitudes the damping rate greatly depends on the oscillation amplitude. The same kind of measurement was repeated for different oscillation amplitudes of the cylindrical tank. In particular, if the oscillation of the free surface was excited below the threshold value, we always found a single exponential decay with a constant decay rate that was independent of the oscillation amplitude.

A completely different behaviour is observed if a surface active material (Kodak Photo-Flo) is added to water in a 1% concentration. In this case the contact angle becomes zero and the damping rate becomes almost constant for every oscillation amplitude in agreement with previous results (Cocciaro *et al.* 1991) obtained for pure octane wetting the solid walls.

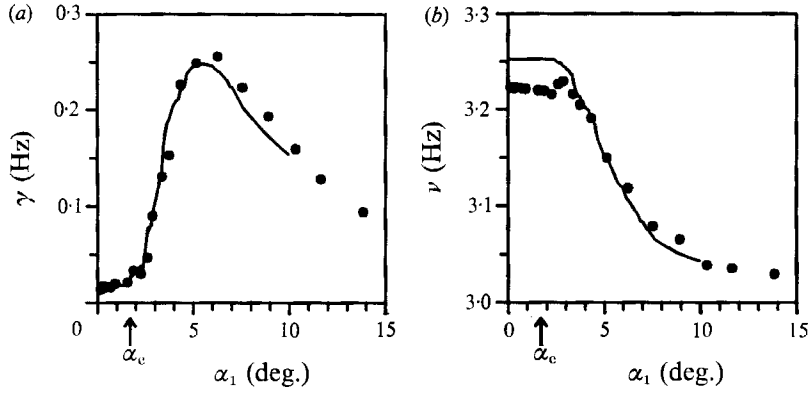

FIGURE 9. (*a*) Dependence of effective damping rate γ on the oscillation amplitude α_1 of the tilt angle. ——, prediction of the boundary-layer approximation in (2.11*a*) for λ given by (3.7) where $D = 0.5$ s/cm and A_c given in figure 3(*a*). (*b*) Dependence of resonance frequency ν on the oscillation amplitude α_1 of the tilt angle. The resonance frequency and the corresponding oscillation amplitude are calculated by making the local best fit of the experimental damped oscillating output signal of the photodetector using the procedure described in the text. ——, prediction of the boundary-layer approximation in (2.11*b*) for $D = 0.5$ s/cm.

Frequency ν and damping coefficient γ versus oscillation amplitude α_1 of the tilt angle are obtained from the experimental points in figure 8 by using the fitting procedure discussed in our previous paper (Cocciaro *et al.* 1991). The experimental values of damping rate γ and oscillation frequency ν versus α_1 are shown in figures 9(*a*) and 9(*b*) respectively.

Two different regimes are seen to exist:

(i) A *low-amplitude regime* ($\alpha < 1°$) where free decay is well represented by a single exponential decay with a constant and very low damping rate $\gamma \approx 15 \pm 2$ mHz and a virtually constant oscillation frequency $\nu \approx 3.222 \pm 0.001$ Hz;

(ii) A *higher-amplitude regime* ($\alpha > 1°$) where both the decay rate and the eigenfrequency are functions of α_1. In this regime the damping rate first increases versus α_1 to reach a maximum value which is ten times higher than that of regime (i) and, then, it decreases.

It is important to note that, although the main features of the damping rate and the eigenfrequency in the high-amplitude regime can always be reproduced by repeating the same kind of measurement on different samples, quantitative differences are often found (up to ≈ 30 mHz). These differences are probably related to difficulties in obtaining identical and uniform boundary conditions after the cleaning procedure.

3.5. *Discussion*

The experimental results in figure 9 can be explained by using the theories of capillary damping discussed in §§2.2 and 2.3. We must distinguish between two different cases.

(i) *Low-amplitude regime* ($\alpha_1 < \alpha_c$)

In this case, the capillary line always remains at rest during the motion of the free surface. This means that $\lambda = 0$ (pinned-end edge condition) and, thus, both the damping coefficient and the eigenfrequency are expected to be independent of the oscillation amplitude (see §2.2) in agreement with the experimental results. If we disregard the possible presence of a thin contaminating film on the free surface, the

damping coefficient and the eigenfrequency are given by (2.12*a*) and (2.12*b*). By solving the 'exact eigenvalue equation' of the Miles theory (1991) and by using the values $g = 980.5$ cm/s^2 and $\lambda_c = 2.7$ mm, we find $\gamma_L = 0$ and $\nu' = 3.255$ Hz. The viscous contributions γ_v and δ_v can be estimated by making the assumption that the Hocking results (1987*a*, *b*) which were obtained for a rectangular channel still hold good for our cylindrical geometry if we substitute the free-end damping rate γ'_w for the rectangular channel with the free-end value γ_w for the cylindrical container. Under this assumption we estimate that $\gamma_v = \delta_v = 0.67\ \gamma_w$. By substituting the cinematic viscosity $\nu_c = 0.0099$ cm^2 s^{-1} at $T = 21$ °C in (2.3) and (2.4) we find $\gamma_v = \delta_v = 0.67\ \gamma_w = 12$ mHz and, thus:

$$\gamma = \gamma_L + \gamma_v = 12 \text{ mHz}; \quad \nu = \nu' - \tfrac{1}{2}\delta_v = 3.249 \text{ Hz}, \tag{3.6}$$

which are close to our experimental values: $\gamma = 15 \pm 2$ mHz and $\nu = 3.222 \pm 0.001$ Hz. However the theoretical value of the eigenfrequency is 27 mHz higher than the experimental one, whilst the theoretical damping rate is 3 mHz lower than the experimental value. In principle, these discrepancies with the theory could be related to the presence of a residual surface contaminating film. For instance, the presence of an inextensible surface film ($C = 1$ in equation (2.13)) is expected to produce a damping rate $\gamma = 0.67\ \gamma_w + \gamma_s = 30$ mHz which is much higher than the experimental value $\gamma = 15$ mHz. However, the precautions taken to avoid surface contamination make this interpretation unlikely, although it is admitted that very low levels of contamination are difficult to detect.

In order to find an alternative explanation of discrepancies between theory and experiment, we must remember that the theoretical values of γ_L and ν' for $\lambda = 0$ were obtained by solving numerically the 'exact eigenvalue equation' (Miles 1991) were *the effects due to static meniscus are disregarded.* According to Miles, the static meniscus is expected to produce corrections to the 'exact eigenvalue equation' of second order in the small parameter $k \approx 0.1$. Since the first-order capillary contribution to the eigenfrequency for $\lambda = 0$ is $\Delta\nu \approx 200$ mHz, we can then expect the static meniscus to produce corrections of the order of $\Delta\nu k^2 \approx 20$ mHz which is precisely of the same order of magnitude as in the experimental discrepancy. Furthermore we remember that the damping rate γ_v and the eigenfrequency $\frac{1}{2}\delta_v$ were obtained by extrapolating to our cylindrical geometry the Hocking results which are valid, in principle, for a rectangular container.

(ii) *Frequency-amplitude regime* ($\alpha_1 > \alpha_c$)

The linear theories in §2.2 clearly predict damping rates and eigenfrequencies which do not depend on the oscillation amplitude of the free surface, in complete disagreement with experimental results. This is also the case of the theory concerning the surface contaminating film (see (2.13)). Therefore we infer that the higher-amplitude regime cannot be explained in terms of these linear theories. According to the experimental results in figure 5(*b*) the capillary coefficient λ in this regime is a real number that increases linearly versus the modulus $|v|$ of velocity of the contact line. According to the theoretical analysis in §2.3 and in Appendix A, we can approximately account for the complex behaviour of the system by defining an effective capillary coefficient

$$\lambda_{\text{eff}} = \frac{2D\omega A_c}{\pi}, \tag{3.7}$$

where $D = 0.5 \pm 0.05$ s/cm is the proportionality coefficient given by the best fit of the experimental points in figure 5(*b*). By substituting the experimental values of A_c

versus α_1 (figure 3a) in (3.7), we obtain the coefficient λ_{eff} versus α_1. Therefore the theoretical values of the damping rate and the eigenfrequency of the first mode for each value of α_1 can be obtained by substituting λ_{eff} for λ in (2.11*a*) and (2.11*b*) and by using (2.12*a*) and (2.12*b*) with $\gamma_v = \delta_v = \gamma_w = 18$ mHz. The full curves in figures 9(*a*) and 9(*b*) represent our theoretical results. The agreement between theory and experiment in both cases is satisfactory if one considers the roughness of the nonlinear model and that no free parameter has been used to draw the theoretical full curves.

4. Conclusions

All the experimental results reported in this paper and in a previous paper about surface gravity waves in the presence of wetting boundary conditions (Cocciaro *et al.* 1991) clearly confirm that the dynamic properties of fluids are greatly affected by the capillary effects occurring near the walls of the container. In particular, the dynamic properties of the contact angle and of the contact line play a fundamental role. Up to now theoretical models have made special assumptions as far as these properties are concerned but, to the best of our knowledge, no direct experimental investigation of the dynamic properties of the contact line has so far been reported for surface gravity–capillary waves. Most experiments on the behaviour of the contact line have dealt with the behaviour of the contact angle in the presence of a steady hydrodynamic flow (see, for instance, Dussan V. 1979). In the present paper, we report a detailed investigation of the dynamic properties of the meniscus and of surface waves when a low viscosity fluid is subjected to a horizontal oscillation at a frequency close to the resonance frequency of the first non-axisymmetric mode. The non-dimensional capillary coefficient λ is measured for the first time and is found to be a real coefficient which is virtually proportional to the velocity of the contact line. In our experiment λ ranges between a minimum value $\lambda = 0$ and a maximum value $\lambda \approx 4$. By generalizing the theory of linear capillary damping in order to account for the nonlinear behaviour of the contact line, we have been able to explain the main experimental results. In spite of considerable approximations made in order to carry out our analytical calculations, a satisfactory quantitative agreement between theory and experiment was found. To the best of our knowledge our results give the first experimental demonstration of the relevance of the capillary mechanism proposed by Miles and Hocking.

We note that the experimental results reported in this paper are fairly general for fluids which do not wet the walls, whilst a completely different behaviour occurs if the fluid wets the vertical walls (Cocciaro *et al.* 1991).

We conclude this short discussion by remarking that the experimental results obtained in this paper have important consequences as far as the nonlinear properties of surface gravity waves are concerned. Miles (1984) theoretically investigated the nonlinear behaviour of surface gravity waves by writing the nonlinear Hamiltonian of surface waves as a power expansion on surface modes truncated at the fourth order. Owing to the nonlinear coupling between the first two resonant modes (longitudinal and transverse mode), critical transitions to stationary, oscillating and chaotic regimes were predicted. Miles assumed that free-end edge conditions were satisfied at the vertical walls and introduced phenomenologically a constant damping coefficient to account for dissipative losses. Nobili *et al.* 1988 investigated the nonlinear behaviour of surface gravity waves in a low viscosity fluid (water) in a cylindrical tank and compared the experimental results with the predictions of the

Miles theory. A satisfactory agreement between theory and experiment was found for very high oscillation amplitudes where the displacement of the capillary line is much higher than the capillary length λ_c and the behaviour of the system tends to approach that predicted by the free-end edge condition. In particular, the phase diagram of the system agreed satisfactorily with the Miles predictions and the geometric shapes of the chaotic attractors were very close to the theoretical ones. On the contrary considerable discrepancies were found at smaller oscillation amplitudes where capillary effects cannot be disregarded and the damping rate cannot be assumed to be a constant coefficient. The experimental results discussed in this paper might explain the origin of these discrepancies.

Our experiment concerns a well-defined fluid and a well-defined geometry of the system. Further experimental work should be devoted to systematically investigating the dynamics of surface waves by changing fluid, temperature, container and geometrical parameters. In particular the dependence of dynamic properties on the product $k_1 \lambda_c$ should be investigated in detail.

This research was supported in part by MPI and in part by CNR (Italy).

Appendix

Boundary condition (2.8) holds good if the contact angle is a linear function of the contact line velocity and no capillary hysteresis is present. The possible effect of the nonlinear behaviour of the dynamic contact angle on the damping of surface gravity waves was investigated theoretically some years also by Miles (1967) using a different theoretical approach. This different approach also provides a simple physical interpretation of the mechanism of capillary damping. Miles assumed that the range of possible static angles is zero, that is the contact line always slides on the vertical walls of the container. Furthermore, according to certain experimental results (Ablett 1923), he assumed that, depending on the value of the hydrodynamic velocity v at the walls of the container, two different dynamic regimes of motion can occur: (i) for $v < v_c$ the contact angle changes as a linear function of the hydrodynamic velocity v of the contact line; (ii) for $v > v_c$ the contact angle becomes independent of the absolute value of velocity v and changes from the minimum value θ_r for the receding fluid and the maximum value θ_a for the advancing fluid. Therefore a Coulomb-like frictional force,

$$F = T[\cos\theta_c(v) - \cos\theta_c], \tag{A 1}$$

acts on the contact between the free surface of the fluid and the vertical walls. The presence of this frictional force acting on the contact line gives a simple physical interpretation of the capillary damping. θ_c is the static contact angle which is assumed to have only one value and $\theta_c(v)$ is the velocity-dependent contact angle. In the region $v < v_c$ Miles assumed the following linear dependence:

$$\cos\theta_c(v) - \cos\theta_c \approx -\xi v/v_c, \tag{A 2}$$

whilst for $v \gg v_c$, Miles assumed that

$$\cos\theta_c(v) - \cos\theta_c \approx \pm\xi = -\xi v/|v|, \tag{A 3}$$

and disregarded the fraction of time during the surface oscillation where the contact angle changes with velocity v (the signs + and − indicate receding and advancing fluid, respectively). Note that, for $\theta_c = \frac{1}{2}\pi$ and $\theta_c(v) - \theta_c \ll 1$, the linear dependence of

(A 2) coincides precisely with the Hocking assumption in (2.6). In particular, if we compare (A 2) with (2.6) and we use (2.7*b*), we find the formal equivalence $\lambda = v_c/\xi\omega\lambda_c$. In order to calculate the capillary damping due to the Coulomb-like frictional force (A 1), Miles makes the implicit assumption that the velocity of the fluid at the contact line is not affected by capillary contributions and, thus, it coincides with the velocity predicted by the free-end edge conditions. Note that, according to (2.8), this assumption is correct only if $\lambda = v_v/\xi\omega\lambda_c \gg 1$. For $v < v_c$ Miles obtained:

$$\gamma_L = \frac{0.245\xi T k_1^2}{\rho v_c} \tanh k_1 h. \tag{A 4a}$$

Using the equivalences $\lambda = v_c/\xi\omega\lambda_c$, $\lambda_c = (T/\rho g)^{\frac{1}{2}}$, $k_1 = 1.841/a$ and

$$\omega_1 = (g k_1 \tanh k^1 h)^{\frac{1}{2}},$$

(A 4*a*) can be written in the alternative form:

$$\gamma_L = \frac{0.451\omega_1 \lambda_c}{\lambda a}. \tag{A 4b}$$

It is interesting to compare (A 4*b*) with (2.11*a*). We find that (2.11*a*) approaches (A 4*b*) for $\lambda \gg 1$. In general, (A 4*b*) overestimates the influence of capillary forces on the damping of surface waves. Indeed, (A 4*a*) was obtained by assuming that the vertical displacement $A_c = \eta(a)$ of the contact line is that given by free-end boundary conditions, whilst the actual vertical displacement of the capillary line is always smaller than that predicted by the free-end edge condition (see (2.8)). In particular, for $\lambda = 0$, η(a) vanishes and (2.11*a*) predicts a zero damping coefficient, whilst (A 4*b*) predicts an infinite damping coefficient.

In the case in which $v \gg v_c$ Miles obtained

$$\gamma_L = \frac{0.398\xi T k_1^2}{\rho\omega_1 A_c} \tanh k_1 h, \tag{A 5}$$

where ω_1 is the resonance angular frequency of the first mode given by (2.2), A_c is the displacement of the fluid at the vertical walls and ξ is related to the experimental values of the receding and advancing contact angles by:

$$\xi = \tfrac{1}{2}|\cos\theta_a - \cos\theta_r|. \tag{A 6}$$

By comparing (A 3) with (2.6) we find the formal equivalence $\lambda = |v|/\xi\omega\lambda_c = D|v|$, where we have defined the coefficient $D = 1/\xi\omega\lambda_c$. This means that the nonlinear regime can be considered as a regime where the value of the capillary coefficient λ is not constant during surface oscillation. As a rough approximation this regime can be described by substituting the actual velocity-dependent capillary coefficient by a constant *effective capillary coefficient*:

$$\lambda_{eff} = \langle\lambda\rangle = D\langle|v|\rangle = \frac{2D\omega A_c}{\pi}, \tag{A 7}$$

where the symbol $\langle|v|\rangle$ denotes the average value of the modulus of the velocity of the contact line over an oscillation period. If we use λ_{eff} given by (A 7) instead of λ in (2.11*a*) we find that (2.11*a*) becomes virtually coincident with (A 5) for $\lambda \gg 1$ (the numerical multiplicative coefficient becomes 0.385 instead of 0.398). According to our previous discussion concerning the linear case, we expect (A 5) to hold good only

if $\lambda = \lambda^{\text{eff}} \gg 1$; we also know that a simple generalization of this equation to the case in which $\lambda < 1$ can be obtained by using the linear formula in (2.11*a*) and (2.11*b*) where coefficient λ is replaced by coefficient λ_{eff} given in (A 7). This new approach allows us to generalize the Miles damping rate in (A 5) to all values of the parameter λ and to make new theoretical predictions as far as the natural frequency is concerned.

REFERENCES

Ablett, R. 1923 An investigation of the angle of contact between paraffin wax and water. *Phil. Mag.* **46**, 244–256.

Benjamin, T. B. & Scott, J. C. 1979 Gravity–capillary waves with edge constraints. *J. Fluid Mech.* **92**, 241–267.

Benjamin, T. B. & Ursell, F. 1954 The stability of the plane free surface of a liquid in vertical periodic motion. *Proc. R. Soc. Lond.* A **225**, 505–515.

Case, K. M. & Parkinson, W. C. 1957 Damping of surface waves in an incompressible liquid. *J. Fluid Mech.* **2**, 172–184.

Cocciaro, B., Faetti, S. & Nobili, M. 1991 Experimental investigation of capillarity effects on surface gravity waves in a cylindrical container: wetting boundary conditions. *J. Fluid Mech.* **231**, 325–343.

Davies, J. T. & Vose, R. B. 1965 On the damping of capillary waves by surface films. *Proc. R. Soc. Lond.* A **286**, 218–234.

Douady, S. 1988 Capillary–gravity surface wave modes in a closed vessel with edge constraint: eigen-frequency and dissipation. *Woods Hole Ocean Inst. Tech. Rep.* WHOI-88-(Sum. Stu. Prog. in GFD).

Douady, S. 1989 Experimental study of the Faraday instability. *J. Fluid Mech.* **221**, 383–409.

Dussan, V., E. B. 1979 On the spreading of liquids on solid surfaces: static and dynamic contact lines. *Ann. Rev. Fluid Mech.* **11**, 371–400.

Dussan, V., E. B., Ramé, E. & Garoff, S. 1991 On identifying the appropriate boundary conditions at a moving contact line: an experimental investigation. *J. Fluid Mech.* **230**, 97–116.

Graham-Eagle, J. 1983 A new method for calculating eigenvalues with application to gravity–capillary waves with edge constraints. *Math. Proc. Camb. Phil. Soc.* **94**, 553–564.

Graham-Eagle, J. 1984 Gravity–capillary waves with edge constraints. D. Phil thesis. University of Oxford.

Hocking, L. M. 1987*a* The damping of capillary–gravity waves at a rigid boundary. *J. Fluid Mech.* **179**, 253–266.

Hocking, L. M. 1987*b* Waves produced by a vertically oscillating plate. *J. Fluid Mech.* **179**, 267–281.

Keulegan, G. H. 1959 Energy dissipation in standing waves in rectangular basins. *J. Fluid Mech.* **6**, 33.

Kitchener, J. A. & Cooper, C. F. 1959 Current concepts in the theory of foaming *Q. Rev. Chem. Soc.* **13**, 71–97.

Lamb, H. 1932 *Hydrodynamics*, 6th edn. Cambridge University Press.

Mei, C. C. & Liu, L. F. 1973 The damping of surface gravity waves in a bounded liquid. *J. Fluid Mech.* **59**, 239–256.

Miles, J. W. 1967 Surface-wave damping in closed basins. *Proc. R. Soc. Lond.* A **297**, 459–475.

Miles, J. W. 1984 Resonantly forced gravity waves in a circular cylinder. *J. Fluid Mech.* **149**, 15–45.

Miles, J. W. 1990 Capillary–viscous forcing of surface waves. *J. Fluid Mech.* **219**, 635–646.

Miles, J. W. 1991 The capillary boundary layer for standing waves. *J. Fluid Mech.* **222**, 197–205.

Miles, J. W. & Henderson, D. 1990 Parametrically forced surface waves. *Ann. Rev. Fluid Mech.* **22**, 143–165.

Nobili, M., Ciliberto, S., Cocciaro, B., Faetti, S. & Fronzoni, L. 1988 Time-dependent surface waves in a horizontally oscillating container. *Europhys. Lett.* **7**, 587–592.

Scott, J. C. 1981 The propagation of capillary–gravity waves on a clean water surface. *J. Fluid Mech.* **108**, 127–131.

Ursell, F. 1952 Edge waves on a sloping beach. *Proc. R. Soc. Lond.* A **214**, 79–97.

Van Dorn, W. G. 1966 Boundary dissipation of oscillatory waves. *J. Fluid Mech.* **24**, 769–779.